Title
HETERONUCLEAR CROSS-POLARIZATION OF SOLID STATE 14N NMR POWDER PATTERNS

Authors
Pratum, T.K.
Klein, M.P.

Publication Date
1983-04-01

Lawrence Berkeley Laboratory
UNIVERSITY OF CALIFORNIA

CHEMICAL BIODYNAMICS DIVISION

Submitted to the Journal of Magnetic Resonance

HETERONUCLEAR CROSS-POLARIZATION OF SOLID STATE ^{14}N NMR POWDER PATTERNS

T.K. Pratum and M.P. Klein

April 1983

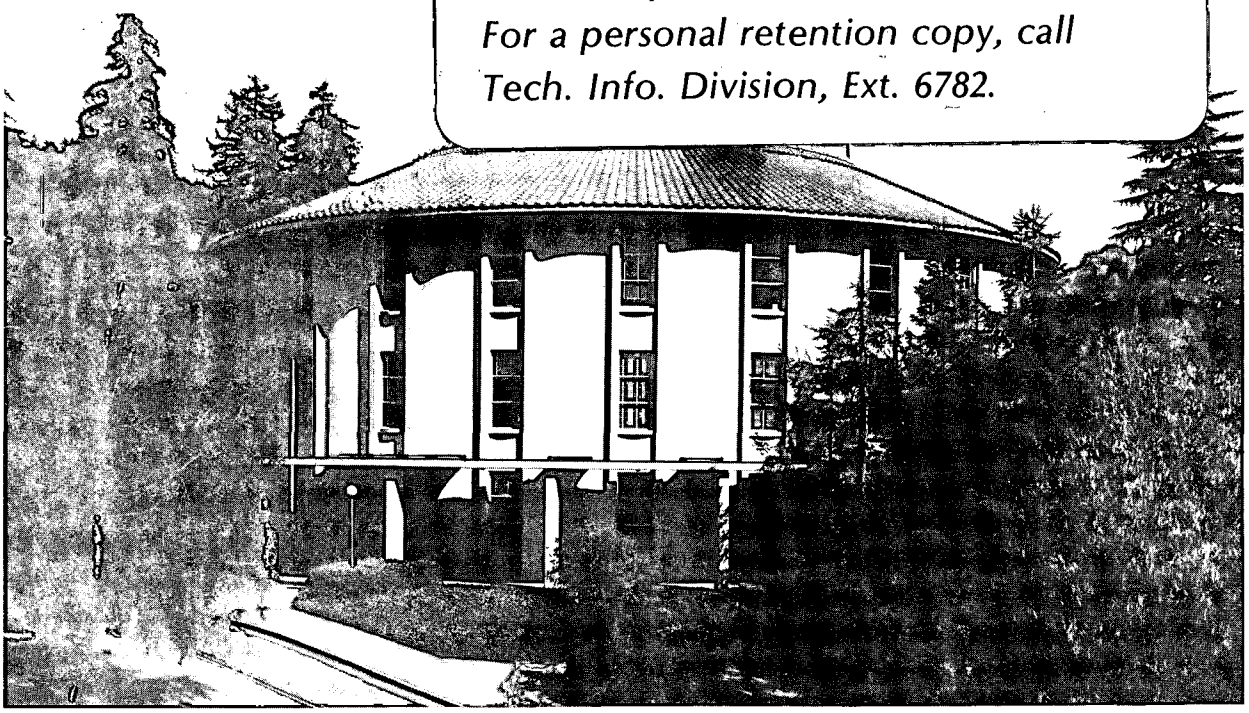

Prepared for the U.S. Department of Energy under Contract DE-AC03-76SF00098

DISCLAIMER

Heteronuclear Cross-Polarization of Solid State ^{14}N NMR Powder Patterns

T. K. Pratum and M. P. Klein

Chemical Biodynamics Division, Lawerence Berkeley Laboratory,

University of California, Berkeley, California 94720

Abstract

The ^{14}N- ^{1}H adiabatic demagnetization in the rotating frame (ADRF) and spin lock cross-relaxation processes are investigated in the regime in which the magnitudes of the radio frequency field (w_1) and quadrupolar interaction (w_Q) are of the same order. The results we observe are the consequence of single ,double and zero quantum effects. The matching condition for various w_Qs is investigated via the effect of the cross relaxation process on the appearance of ^{14}N NMR powder spectra. It is found that a simple, but accurate, treatment of the ^{14}N three level system in terms of two matching conditions gives reasonable agreement with the experimental results.

Introduction

The importance of nitrogen to the chemical world cannot be overstated. Unfortunately the most abundant isotope, ^{14}N, has both a large quadrupole moment and a low gyromagnetic ratio, making it quite unattractive from an NMR spectroscopists perspective. Nonetheless, interesting information has been determined by observing the ^{14}N quadrupolar interaction in single crystals (1-4), powders (5), and partially ordered phases (6-9).

Although the magnitude of the electric field gradients surrounding nitrogen nuclei in many interesting molecules will make the observation of a quadrupolar broadened powder spectrum nearly impossible, there do exist a significant number of symmetrically substituted ammonium compounds which have quadrupolar coupling constants which are on the same order as those observed for deuterium compounds (5). Observation of these broadened NMR powder lineshapes may be facilitated by the use of quadrupolar echo (10), multiple frequency excitation (11), or the interpretation of sideband spectra from magic angle spinning experiments(12). From a rigid lattice powder lineshape one can determine the quadrupole coupling constant (e^2qQ) and asymmetry parameter (η) once distortions inherent to the particular technique have been taken into account.

Low S/N can be considered an integral part of any powder lineshape; the broader the line the lower its intensity at any given point. For ^{14}N, this problem is compounded by a low gyromagnetic ratio. A technique which has clearly been demonstrated as a valuable method for enhancing NMR signals of weakly resonating nuclei is that of rotating frame cross-

polarization (13). In particular those schemes which involve direct detection of the polarized spin signal will give the most undistorted representation of its frequency domain intensity (14). Here we investigate the effect of applying the direct detection cross-polarization technique to broad distributions of ^{14}N quadrupolar frequencies in an attempt to see if the technique has any practical utility under these circumstances. This work complements that of Brunner, Reinhold and Ernst (15,16) in which the indirectly detected double quantum cross-polarization of this nucleus in single crystals was investigated.

The Cross-Polarization Process

The dynamics of the cross-polarization process have been deduced by many in the past (17,18), a particularly enlightening analysis relating to our present situation is given by Vega et al (19). No attempt is made here toward an exact treatment; we merely show a qualitative understanding of the results we have obtained.

A typical proton-nitrogen cross-polarization experiment consists of three parts: (1) preparation of the proton polarization, (2) establishment of contact between the proton and nitrogen spins, and (3) observation of the nitrogen polarization produced. The preparation phase involves transfer of the large proton Zeeman polarization to a much smaller effective field via an adiabatic demagnetization in the rotating frame (ADRF), or spin lock (SL). Contact is established through the heteronuclear dipolar interaction when the possibility of mutual, energy conserving spin flips exists. This is tantamount to matching the

nitrogen and proton effective fields in the rotating frame. In our experiments, the nitrogen polarization is observed directly by use of a quadrupolar echo, or with additional pulses being applied to the system in order that non-observable double quantum coherence be rendered observable.

Contact Phase of the Cross Polarization

Prior to the establishment of contact between the proton (I) and nitrogen (S) spins, it is assumed that the S spins are saturated and will exhibit no signal. During the contact phase, the assumption of a spin temperature in the rotating frame is assumed to be valid for both the I and S spins, and establishment of a purely thermodynamic equilibrium between the two systems occurs. The variation of the inverse S spin temperature with time, assuming no coupling to the lattice (i.e. $T_{1\rho}=\infty$, $T_{1D}=\infty$) follows (20):

$$\beta_s = \beta_{eq}(1-\exp[-(1+\epsilon\eta^2)t/T_{IS}] \qquad [1]$$

where $\beta_{eq}=\beta_I/1+\epsilon\eta^2$, $\eta=w_{es}/w_{ei}$ and $\epsilon=[N_S S(S+1)]/[N_I I(I+1)]$. With a full treatment of the dynamics (17), one can explicitly derive T_{IS} via:

$$T_{IS}^{-1} = \mathrm{Tr}\,[H_S]^{-2}\int dt\,\mathrm{Tr}\,([H_{IS},H_S]\exp(-i(H_S+H_I)t)$$

$$x[H_{IS},H_S]\exp(i(H_S+H_I)t)), \qquad [2]$$

but we will merely take over the results of Vega et al (19)

$$T_{IS}^{-1} = 1/2\ M_{2IS}\ J_z(w_{es} - w_{ei}) \qquad [3]$$

for the SL case, and

$$T_{IS}^{-1} = M_{2IS}\ J_x(w_{es}) \qquad [4]$$

for the ADRF case. In these expressions, w_{ei} and w_{es} are the rotating frame effective fields of the I and S spins respectively, M_{2IS} is the dipolar second moment of the S spins due to the I spins and is defined

$$M_{2IS} = Tr[H_{IS},H_S]^2/Tr[H_S]^2. \qquad [5]$$

The spectral density $J_p(w)$ is defined

$$J_p(w) = \int \cos wt\ C_p(t)dt; \quad p=x, \text{ or } z \qquad [6]$$

where $C_p(t)$ is the autocorrelation function of the I spins due to homonuclear dipolar flip-flop processes. It is to be noted that this will differ between ADRF and SL states due to the truncation of the II spin interaction in the latter (when the irradiation field exceeds the local field).

The cross-polarization process is expected to distort a powder lineshape, composed of contributions from crystallites at all possible orientations with respect to the high field, because the cross relaxation rate is orientation dependent. In particular, both the heteronuclear and homonuclear dipolar interaction possess a $P_2(\cos\theta)$ dependence, and thus it is expected that both M_{2IS} and $J_p(w)$ will have a similar dependence. Previous observations of distortions in chemical

shift powder patterns have been attributed to the variation of M_{2IS} across the spectral line (14). In the intermediate r.f. field amplitude region in which we work, the rotating frame effective field of the nitrogen spins (w_{es}) will exhibit a large dependence on quadrupolar frequency. This will cause the ^{14}N rotating frame heat capacity and the point at which the spectral density function is sampled to vary across the powder pattern. In this treatment, we will concentrate only on the distorting effect of the rotating frame effective field and ignore that of M_{2IS} and $J_p(w)$. Justification for this simple approach is provided by its sufficiency in explaining our results.

Rotating Frame Effective Fields

Derivation of the rotating frame effective field for a spin one nucleus has been carried out by several authors (21,22). We will treat this briefly one more time with a focus toward the regime of w_{1S} on the order of w_Q.

The rotating frame Hamiltonian of a spin one nucleus experiencing a first order quadrupolar interaction is given as

$$H_S = -\Delta w S_z - w_{1S} S_x + w_Q/3(3S_z^2 - S(S+1)) \qquad [7]$$

where $w_Q = 3/4\ e^2qQ/h(1/2(3\cos^2\theta - 1) + \eta\sin^2\theta\cos 2\phi)$, $w_{1S} = \gamma_S H_{1S}$, and $\Delta w = \gamma H_o - w$. With the assumption $\Delta w = 0$ and conversion to fictitious spin 1/2 operators (22), [7] becomes

$$H_S = -\sqrt{2} w_{1S}(S_x^{1-2} + S_x^{2-3}) + 2w_Q/3(S_z^{1-2} - S_z^{2-3}). \qquad [8]$$

This equation is now put in diagonal form via $U^\dagger H_S U = H_S^T$ (the superscript

T refers to a tilted operator) where

$$U=\exp(i\frac{\pi}{2}S_y^{1-3})\exp(-i\,\theta\,S_y^{2-3}),$$

$$\theta=\text{atan}(2w_{1S}/w_Q), \text{ and}$$

$$H_S^T=-(4w_{1S}^2+w_Q^2)^{1/2}S_z^{2-3}+w_Q/3(S_z^{1-3}+S_z^{1-2})$$

$$=-w_eS_z^{2-3}+w_Q/3(S_z^{1-3}+S_z^{1-2}). \qquad [9a]$$

For small resonance offsets ($\Delta w<<w_{1s}$), the term w_e is modified to

$$w_e=(4w_{1S}^2+4\,\Delta w^2+w_Q^2)^{1/2}.$$

Equation [9a] can now be rearranged, taking advantage of the relation $S_z^{1-3}=S_z^{1-2}+S_z^{2-3}$, to give two degenerate expressions

$$H_S^T=-(w_e-w_Q)/2S_z^{1-3}-(2/3w_Q+(w_e-w_Q)/2)(S_z^{2-3}-S_z^{1-2}), \text{ and} \qquad [9b]$$

$$=(w_e+w_Q)/2S_z^{1-2}+(2/3w_Q-(w_e+w_Q)/2)(S_z^{1-3}+S_z^{2-3}). \qquad [9c]$$

The eigenvalues of this Hamiltonian are plotted in Figure 1a as a function of w_Q. The three rotating frame energy splittings (effective fields) are: w_e , $(w_e-w_Q)/2$, and $(w_e+w_Q)/2$.

Hartmann- Hahn Conditions

To easily derive the Hartmann-Hahn conditions, we will use an argument similar to that of Vega (23). In order for the perturbation

H_{IS} to provide a path for polarization transfer between the I and S spins, it must become nonsecular over this manifold. The modulation of the heteronuclear dipolar interaction H_{IS} by the I and S effective fields provides a means for this to occur. Determination of the Hartmann-Hahn conditions reduces to determining the effect of H_S^T on H_{IS}.

In terms of fictitious spin 1/2 operators,

$$H_{IS} = 4\sum_i b_i I_{zi} S_z$$

where we consider the contact of a single spin S with many I spins, and $b_i = \gamma_I \gamma_S h/r_i^3(3\cos^2\theta_i - 1)$. Straightforward transformation of this into the tilted frame via $U = \exp(i\frac{\pi}{2} I_y)\exp(i\frac{\pi}{2} S_y^{1-3})\exp(-i\theta S_y^{2-3})$ yields

$$H_{IS}^T = U^\dagger H_{IS} U = 4\sum_i b_i I_{xi}(\cos\frac{\theta}{2} S_x^{1-3} + \sin\frac{\theta}{2} S_x^{1-2}). \qquad [10]$$

We now wish to find the effect of the Hamiltonian

$$H_I^T + H_S^T = -w_{1I} I_z - w_e S_z^{2-3} + w_Q/3(S_z^{1-3} + S_z^{1-2}) \qquad [11]$$

on H_{IS}^T. The I spins, which possess a spin of 1/2, will modulate the term I_z in H_{IS}^T with a frequency $w_{1I} = \gamma_I H_{1I}$. For the S spins we must calculate

$$H_{IS}^{ST}(t) = \exp(-iH_S^T t)\, H_{IS}^{ST} \exp(iH_S^T t)$$

$$= \exp(-iH_S^T t)\,(\cos\frac{\theta}{2} S_x^{1-3} + \sin\frac{\theta}{2} S_x^{1-2})\exp(iH_S^T t) \qquad [12]$$

where H_{IS}^{ST} refers to the tilted S spin portion of H_{IS}^T, and $H_S^T = -w_e S_z^{2-3} + w_Q/3(S_z^{1-3} + S_z^{1-2})$. This yields the result

$$H_{IS}^{ST}(t) = \cos\theta/2(\cos[(w_e - w_Q)t/2]S_x^{1-3} - \sin[(w_e - w_Q)t/2]S_y^{1-3})$$

$$+\sin\theta/2(\cos[(w_e + w_Q)t/2]S_x^{1-2} + \sin[(w_e + w_Q)t/2]S_y^{1-2}) \qquad [13]$$

in which it is clear from equations [9b] and [9c] that only the fields $-(w_e-w_Q)/2$ along S_z^{1-3} and $(w_e+w_Q)/2$ along S_z^{1-2} are effective in cross-relaxation. The Hartmann-Hahn matching conditions are

1. $w_{1I}=(w_e - w_Q)/2$, and

2. $w_{1I}=(w_e + w_Q)/2$.

When $w_Q=0$, both reduce to $w_{1I}=w_{1S}$, and when w_Q is much larger than w_{1S}, condition 1 becomes $w_{1I}=w_{1S}^2/w_Q$ (19). Conditions 1 and 2 are plotted as a function of w_Q in Figure 1b.

Relaxation due to condition 1 occurs along S_z^{1-3} in the tilted frame and will have a relaxation rate, for the ADRF case,

$$T_{IS}^{-1} \propto \cos^2\frac{\theta}{2} J_x((w_e - w_Q)/2), \qquad [14]$$

while that due to condition 2 occurs along S_z^{1-2} and is characterized by

$$T_{IS}^{-1} \propto \sin^2\frac{\theta}{2} J_x((w_e + w_Q)/2). \qquad [15]$$

Since the two effective fields are opposite in sign, full overlap of conditions 1 and 2 (i.e. when $w_{1I}=w_{1S}$, and $w_{1S}>>w_Q$) results in a polarization along S_z^{2-3} in the tilted frame which is characterized by

$$T_{IS}^{-1} \propto J_x(w_e/2). \qquad [16]$$

Partial overlap of conditions 1 and 2 produces a complicated situation

which we shall not attempt to analyze here.

Polarizations Produced

It is now necessary to rotate each polarization produced in the tilted frame back to the original frame of reference. Rotation of S_z^{1-3} produces an observable coefficient S_x of $\sin\theta = 2w_{1S}/w_e$, while rotation of S_z^{1-2} produces an observable coefficient S_x of $-\sin\theta$. In the case of full overlap, the rotation of S_z^{2-3} generates only S_x (because θ must be nearly 90°). The remainder of the polarization in each case lies in $[3S_z^2-S(S+1)]/2$ (zero quantum order) and $[S_x^2-S_y^2]/2$ (double quantum order), The proportion of double and zero quantum coherence is dependent upon the matching condition. Condition 1 leads to a preponderance of double quantum order, and condition 2 to zero quantum order; when w_Q is much larger than w_{1S}, condition 1 becomes a purely double quantum matching condtion and condition 2 becomes purely zero quantum. The double quantum coefficient is rendered observable via a hard ($w_{1S}>>w_Q$) 90° pulse 45° out of phase with the mixing period, or alternatively, it may be observed with one half the efficiency via a hard 45° pulse 90° out of phase with the mixing period (19). At $w_Q=0$, only a coefficient of S_x is produced regardless of the matching condition, as would be expected.

Experimental Considerations

In order to test the usefulness of the cross polarization scheme experimentally, we chose ammonium sulfate, a compound which had been well characterized in the past. Its room temperature crystal structure

gives rise to two non-equivalent nitrogen nuclear sites with the following quadrupolar couplings (24)

site I: e^2qQ/h=154.55 kHz, η =0.684

site II: e^2qQ/h=115.71 kHz, η =0.749.

A standard proton decoupled quadrupolar echo spectrum is shown in Figure 2. This compound is convenient for study due to its long proton $T_{1\rho}$ (>80 msec) and T_{1D} (>1 sec) at room temperature.

In order to observe the effect of cross relaxation on such a broad spectrum (230 kHz), it is necessary to echo the single and double quantum polarizations produced. Outlines of the r.f. fields we have used for this purpose are shown in Figure 3. A quadrupolar echo sequence consists of a 90° pulse of the same phase as the mixing field. This will only echo observable coefficients present following the cross polarization. Non-observable double quantum polarization is rendered observable via a 90° pulse of 45° phase, this observable may now be echoed by a 90° pulse in phase with the mixing field as shown in figure 3. After such a sequence, we ideally expect to observe three echo signals; two stimulated echoes of single quantum origin and one double quantum echo which will appear as a derivative. This will be discussed at length later.

Experimental Procedure

All experiments were performed on a home built spectrometer operating at a ^{14}N resonance frequency of 19.507 MHz (26). Control of

the spectrometer is provided by a Nicolet Instument Corporation 1180 computer and 293B programmable pulser. Nicolet software (NTCFTB) was used with only very minor modification. Data were digitized on a Nicolet Explorer IIIa digital oscilloscope having a maximum data acquisition rate of 50 ns/point. All data were acquired in the presense of proton decoupling.

The ammonium sulfate was of reagent grade and used without further purification. Tetraalkylammonium compounds were recrystallized at least once from an appropriate solvent. All compounds had been subjected to drying in vacuo at 85° C for at least 12 hours prior to being sealed in 5mm glass tubes in an argon dry box.

Observed Echo Signals

The single quantum sequence of Figure 3 is expected to generate a single echo which, when fourier transformed, will give us the single quantum frequency response of the system. In order to observe the double quantum response of the system, we have chosen the more efficient 45° out of phase pulse sequence, and this sequence is expected to create three echoes. The first occurs τ_1 following the second pulse and is the result of observable x magnetisation being stored along z during τ_2 due to the 45° out of phase pulse at τ_1. The next echo is expected to occur at $\tau_2 - \tau_1$ and is the stimulated echo of the observable x magnetisation (reduced by a factor $\sqrt{2}/2$). The final echo occurs at τ_2 and is due to magnetisation created by the pulse at τ_1: double quantum coherence (reduced, in this case, also by $\sqrt{2}/2$). In Figure 4a we observe three echoes, but they occur at $\tau_2 - \tau_1$, τ_2, and $\tau_2 + \tau_1$. The echo predicted

to occur at τ_1 has been subtracted out by the phase cycling technique used in order to minimize transient instrument response caused by the final echo pulse. The echo at τ_2 manifests a derivative character, clearly showing it as the double quantum echo. We observe an unpredicted echo at $\tau_2+\tau_1$. In order to enlighten us on this matter, a computer simulation was performed in which an initial density matrix is populated in accordance with exponential relaxation along the two matching conditions, carried through an evolution corresponding to our experimental pulse sequence, and integrated over a weighted distribution of quadrupolar frequencies to give a time domain response signal. The result, in 4b, shows that the echo at $\tau_2+\tau_1$ is indeed predicted theoretically. Further calculations have shown that it will disappear when echo pulses whose amplitudes far exceed the largest quadrupolar frequency present are used. This echo is therefore attributed to the fact that our pulses are not performing simple rotations on the system.

In the double quantum experiment, illustrated in Figure 3, it is generally desirable to eliminate all but the double quantum echo. This can be satisfactorly approached in the following manner. The echo at τ_1 follows the phase of the final pulse (so long as the mixing field and first pulse phase are held constant) and is easily subtracted out as we mentioned previously; but this echo can easily be moved away from the double quantum echo by making τ_1 short, and so presents no problems. The stimulated echo can be suppressed and the echo at $\tau_2+\tau_1$ made to cancel by the following sequence: [(mixing field phase, first pulse phase, second pulse phase)] (45,0,90) add, (45,180,90) subtract. The stimulated echo does not occur for the same reason that two pulses of the same phase do not produce a quadrupolar echo from a system

intitially characterized by a Zeeman polarization. The echo at $\tau_2+\tau_1$ is subtracted away as it always follows the phase of the mixing field. The echo at τ_1 depends upon the phase of both the mixing field and the second pulse and does not cancel in this sequence. The double quantum echo will appear entirely in the quadrature channel, and 100% of this polarization is echoed by this sequence (in the limit that we have ideal pulses). Also, all pulses and mixing periods may be cycled through 90° phase increments in order to equalize the two channels in quadrature phase operation. Figure 4c shows the experimental result of this sequence. Indeed now the double quantum echo is easily separated from the rest by left shifting.

Width of the Cross Polarization

Upon fourier transformation of the second half of the aforementioned echoes, we will obtain a frequency domain spectrum which will always consist of two lobes; except for the single quantum situation $w_{1I}=w_{1S}$ where the center of the spectrum is enhanced. The intensity of the double quantum echo will always vanish at $w_0=0$ as double quantum coherence cannot exist at this point. The width of the lobes may be dependent upon several factors: which condition is matched (or, which operator is populated in the tilted frame), the single or double quantum nature of the polarization produced, and the width of the spectal density function.

Effect of the Matching Condition

In Figure 5 we show single quantum frequency domain spectra as a

function of proton r.f field amplitude using the spin lock experiment. Solving the matching conditions for w_Q, we find that, for fixed w_{1I} and w_{1S} we should have rotating frame effective field equality between the I and S spins at

$$w_Q=(w_{1S}^2- w_{1I}^2)/w_{1I} \qquad [17]$$

for condition 1, and

$$w_Q=(w_{1I}^2- w_{1S}^2)/w_{1I} \qquad [18]$$

for condition 2. It is observed that the separation of the two lobes decreases with increasing w_{1I} in accordance with equation [17]. As w_{1I} is increased above w_{1S}, the lobes once more separate and follow the relation [18]. The rapid degadation of the S/N with increasing w_{1I} is easily understood by examining the relationship defining T_{IS}^{-1} for this matching condition. The $\sin^2 \frac{\theta}{2}$ factor (see equation [15]) will decrease precipitously toward zero as w_Q is increased, and for this reason this matching condition is of no practical interest in the enhancement of large quadrupolar splittings. This is another way of stating the fact that the heteronuclear dipolar interaction is ineffective for the zero quantum transition.

A very important difference between the two matching conditions is readily seen in Figure 1b. For large w_Q, condition 1 has a very small negative slope (i.e. it becomes nearly independent of w_Q), while condition 2 has a very large positive slope. This causes spectra due to relaxation according to condition 1 to tail off toward large w_Q, and that due to condition 2 to have a sharp cutoff at large w_Q. The best advantage may be taken of condition 1 in the ADRF experiment where it

has the effect of broadening the cross-polarization greatly (we can reduce w_{1S} to move into a region where the slope of the matching condition is smaller). We should mention that the observed difference between SL and ADRF experiments (see Figure 6) could also be due to a broader spectral density for the ADRF, but we can simulate both the ADRF and SL experiments using nearly the same dipolar correlation time .

Single vs. Double Quantum Echoes

Figure 7 shows the resulting fourier transformation of single quantum and double quantum echoes. As expected, the double quantum echo has greater S/N overall, and much greater response in the wings of the spectrum. Of course, there is also a correspondingly lesser response near the center (at frequencies less than $2w_{1S}$). The full width of the cross polarization is best realized by observing the double quantum response.

It should be emphasized that we have applied non-ideal pulses to the system in order to rotate non-observables into observables and to echo the observables. The single quantum echo sequence merely has a single non-ideal pulse, while the double quantum echo sequence has two non-ideal pulses applied and will have its large large quadrupolar frequencies attenuated to a greater degree. Thus it is very difficult experimentally to observe the full frequency response of the double quantum echo.

Unfortunately, the spectrum will always suffer some distortion even for infinitely long cross polarization times because the heat capacity

of the nitrogen spins varies across the powder pattern. The result of this for condition 1 is that the center of the spectrum is always preferentially enhanced even though the T_{IS} in the wings may be shorter. This fact is demonstrated in Figure 8.

Practical Considerations

The general utility of this technique is illustrated in Figure 9 where we have plotted the cross polarized spectra of three tetraalkylammonium compounds. None of these compounds would yield a reasonable spectrum in a finite amount of time without cross-polarization due to exceedingly long T_1s. From the preceeding discussion, the relevent experimental considerations should be obvious. When attempting to cross-polarize a fairly narrow distribution it is most feasible to match $w_{1I}=w_{1S}$ with each being as large as possible. For powder patterns of any breadth, one should decrease w_{1I} below w_{1S}, and even use ADRF if T_{1D} allows. In the latter case, most of the signal appears in the double quantum echo and, upon fourier transformation, yields a totally asymmetric spectrum. If necessary, this can be overcome via a magnitude calculation or preferably integration of the fid prior to fourier transformation. It is always possible to obtain substantial signal enhancement in the single quantum echo, but this requires increased w_{1S}, decreasing the breadth of the cross polarization and increasing the instrumental demands. In cases where both $T_{1\rho}$ and T_{1D} are sufficiently long, it best to view the center of a broad line via a single quantum SL experiment with $w_{1I}=w_{1S}$ and the wings via a double quantum ADRF experiment.

Acknowledgements

We would like to thank Drs. Jim Murdoch and Joel Garbow, and Professor Alex Pines for helpful discussions. This work has been supported by the Office of Energy Research, Office of Health and Environmental Research, Health Effects Research Division of the U.S. Department of Energy under contract DE-AC03-76SF00098.

References

1. E. K. Wolff, R. G. Griffin and C. Watson, J. Chem. Phys. 66,12,5433 (1977).

2. R. E. Stark, R. A. Haberkorn and R. G. Griffin, J. Chem. Phys. 68,4,1996 (1978).

3. G. Bodenhausen, R. E. Stark, D. J. Ruben and R. G. Griffin, Chem. Phys. Lett. 67,2,424 (1979).

4. R. A. Haberkorn, R. E. Stark H. van Willigen and R. G. Griffin, J. Am. Chem. Soc. 103,2534 (1981).

5. T. K. Pratum and M. P. Klein, J. Magn. Reson. (1983) in press.

6. D. J. Siminovich, M. Rance and K. R. Jeffrey, FEBS Lett. 112,1 (1980).

7. T. M. Rothgeb and E. Oldfield, J. Biol. Chem. 256,12,6004 (1981).

8. D. J. Siminovich and K. R. Jeffrey, Biochem. Biophys. Acta. 645,270 (1981).

9. P. Eriksson, A. Khan, and G. Lindblom, J. Phys. Chem. 86,387 (1982).

10. J. H. Davis, K. R. Jeffrey, M. Bloom, M. I. Valic and T. P. Higgs, Chem. Phys. Lett. 42,2,390 (1976).

11. D. E. Wemmer, E. K. Wolff and M. Mehring, J. Magn. Reson. 42,460 (1981).

12. M. Matti Maricq and J. S. Waugh, J. Chem. Phys. 70,7,3300 (1979).

13. S. R. Hartmann and E. L. Hahn, Phys. Rev. 128,5,2042 (1962).

14. A. Pines, M. G. Gibby and J. S. Waugh, J. Chem. Phys. 59,2,569 (1973).

15. P. Brunner, M. Reinhold and R. R. Ernst, J. Chem. Phys. 73,3,1086 (1980).

16. M. Reinhold, P. Brunner, and R. R. Ernst, J. Chem. Phys. 74,1,184 (1981).

17. D. A. McArthur, R. E. Walstedt and E. L. Hahn, Phys. Rev. 188,2,609 (1969).

18. D. E. Demco, J. Tegenfeldt and J. S. Waugh, Phys. Rev. B, 11,11,4133 (1975).

19. S. Vega, T. W. Shattuck and A. Pines, Phys. Rev. A, 22,2,638 (1980).

20. R. T. Schumacher, Phys. Rev. 112,3,837 (1958).

21. S. Vega and A. Pines, J. Chem. Phys. 66,12,5624 (1977).

22. S. Vega, J. Chem. Phys. 68,12,5518 (1979).

23. S. Vega, Phys. Rev. A, 23,6,3152 (1981).

24. L. S. Batchelder and J. L. Ragle, J. Magn. Reson. 37,469 (1980).

25. M. Bloom, J. H. Davis and M. I. Valic, Can. J. Phys. 58, 1510 (1980).

26. W. C. Shih, Ph.D. thesis U. C. Berkeley (1979).

Figure captions

1. (a)The rotating frame energy levels of a spin one nucleus experiencing r.f. irradiation as a function of its first order quadrupolar interaction (w_Q). The energies correspond to the eigenvalues of the Hamiltonian equation [7]. The eigenstates x,y, and z are defined as follows:

$$|X\rangle = \sqrt{2}/2\ (|+1\rangle - |-1\rangle),$$

$$|Y\rangle = \sqrt{2}/2\cos\frac{\theta}{2}|+1\rangle - \sin\frac{\theta}{2}|0\rangle + \sqrt{2}/2\cos\frac{\theta}{2}|-1\rangle, \text{ and}$$

$$|Z\rangle = \sqrt{2}/2\sin\frac{\theta}{2}|+1\rangle + \cos\frac{\theta}{2}|0\rangle + \sqrt{2}/2\sin\frac{\theta}{2}|-1\rangle$$

where $\theta = \text{atan}(2w_{1S}/w_Q)$. (b)Hartmann-Hahn matching conditions 1 and 2 as a function of w_Q.

2. A room temperature proton decoupled quadrupolar echo spectrum of ammonium sulfate. This signal is the result of 3000 acquisitions using 3.7 usec 90° pulses and an 80 usec interpulse delay. The dotted line represents the rigid lattice spectrum calculated on the basis of the quadrupole coupling parameters given in the text, convolved with 800 Hz of lorentzian linebroadening, and multiplied by a function which accounts for the finite duration of the excitation and echo pulses (25).

3. A schematic representation of the cross-polarization quadrupolar echo sequences. In the two experiments at the top of the figure, the proton polarization is prepared via an adiabatic demagnetization in

the rotating frame (ADRF), while those at the bottom use a spin lock (SL). The left side of the figure uses a single pulse to elicit a single quantum quadrupolar echo. In order to observe the double quantum response, a pulse is inserted between the mixing period and the echo pulse as depicted on the right side of the figure. In our experiments, all pulses are of 90° and ϕ in the double quantum experiment is 45°. In all sequences, the ^{14}N polarization is monitored directly during the period following the echo pulse.

4. (a)The experimental result of the double quantum SL experiment on ammonium sulfate. A 43 kHz ^{14}N r.f. field, 24 kHz ^{1}H r.f. field and 3.5 usec 90° pulses were used to elicit this response. The first delay τ_1 was 80 usec and the second delay τ_2 was 140 usec. The phases were cycled (180,225,180)add, (0,45,180)subtract, where (mixing field phase, first pulse phase, second pulse phase); this entire sequence was phase shifted 90° every third time it was executed in order to equalize the two channels of the quadrature phase detector. (b)Calculated response to the experimental parameters in (a); a gaussian spectral density function with a correlation time of 400 usec was used. (c)The experimental result of the double quantum SL experiment using the same parameters as (a), but here the phases were cycled (45,0,90)add, (45,180,90)subtract.

5. Frequency domain response of the single quantum SL experiment as a function of proton r.f. field amplitude for ammonium sulfate. The sequence used a ^{14}N r.f. field amplitude of 33 kHz, 2 msec mixing time, a 3.5 usec 90° pulse and a τ of 100 usec. Each spectrum is the result of 800 acquisitions with 800 Hz of lorentzian linebroadening.

6. SL and ADRF double quantum frequency domain spectra of ammonium sulfate. In each case a 2 msec mixing period was followed by a D.Q. echo sequence using 3.5 usec 90° pulses, a τ_1 of 80 usec and a τ_2 of 140 usec. For the SL experiment the ^{14}N r.f. field amplitude was 43 kHz, and that of the protons was 23 kHz; while for the ADRF experiment the ^{14}N r.f. field amplitude was 18.5 kHz. Each spectrum is the result of 1600 acquisitions with 800 Hz of lorentzian linebroadening.

7. Frequency domain response of single quantum (S.Q.) and double quantum (D.Q.) echoes for ammonium sulfate. Proton order was established via an ADRF. The ^{14}N r.f. field amplitude was 8 kHz, mixing time was 2 msec, and 3.5 usec 90° pulses were used. For the S.Q. case, τ was 140 usec, while for the D.Q. case τ_1 was 80 usec and τ_2 was 140 usec. These signals are each the the result of 1200 acquisitions with 800 Hz of lorentzian linebroadening. The two inner inflection points of this powder pattern occur at 10.9 kHz and 18.3 kHz respectively.

8. The effect of the mixing time upon the double quantum frequency domain spectrum of ammonium sulfate. The double quantum ADRF experiment was used with a 8 kHz ^{14}N r.f. field amplitude, 3.5 usec 90° pulses, a τ_1 of 80 usec and a τ_2 of 140 usec. Each spectrum is the result of 1200 acquisitions with 800 Hz of lorentzian linebroadening applied.

9. Cross polarized ^{14}N spectra of three tetraalkylammonium compounds. In all cases the single quantum echo response is given.

(a)Tetrabutylammonium bromide at -60° C. This signal is the result of a 200 acquisition spin lock experiment in which the ^{14}N and ^{1}H r.f. field amplitudes were matched at 50 kHz. A 2 msec mixing time was followed by a 90 usec delay and a 5 usec 90° pulse. The dotted line represents a powder pattern with e^2qQ/h= 24.4 kHz and η = 0.55, convolved with 200 Hz of lorentzian linebroadening and multiplied by a function to account for the finite duration of the single echo pulse. (b)Tetraethylammonium iodide at -90° C. This signal is the result of a 280 acquisition ADRF experiment in which the ^{14}N r.f. field amplitude was 26 kHz. A 10 msec mixing time was followed by an 80 usec delay and a 3.5 usec 90° pulse. The dotted line represents a powder pattern with e^2qQ/h=42.3 kHz and η =0.0 convolved with 300 Hz of lorentzian linebroadening, and multiplied by a function to account for the finite duration of the single echo pulse. (c)Tetrapropylammonium iodide at -90°C. This signal is the result of a 400 acquisition ADRF experiment in which the ^{14}N r.f. field amplitude was 29 kHz. A 5 msec mixing time was followed by an 80 usec delay and a 3.5 usec 90° pulse. The dotted line represents a powder pattern with e^2qQ/h=102 kHz and η =0.55, convolved with 800 Hz of lorentzian linebroadening and multiplied by a function to account for the finite duration of the single echo pulse. A double quantum experiment at larger r.f. field amplitude was also run in order to clearly delineate the shoulders of the powder pattern and better define the quadrupole coupling parameters.

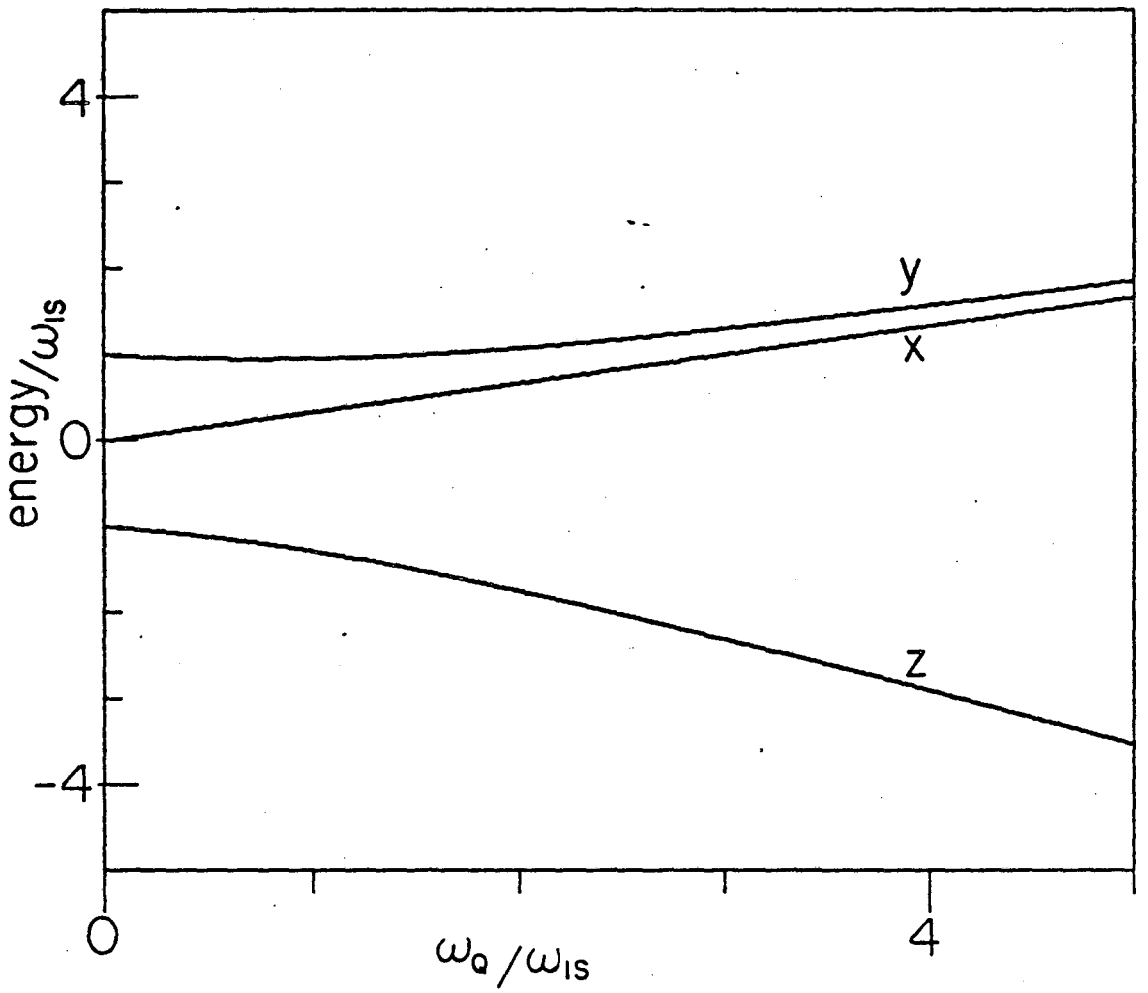

Figure 1a

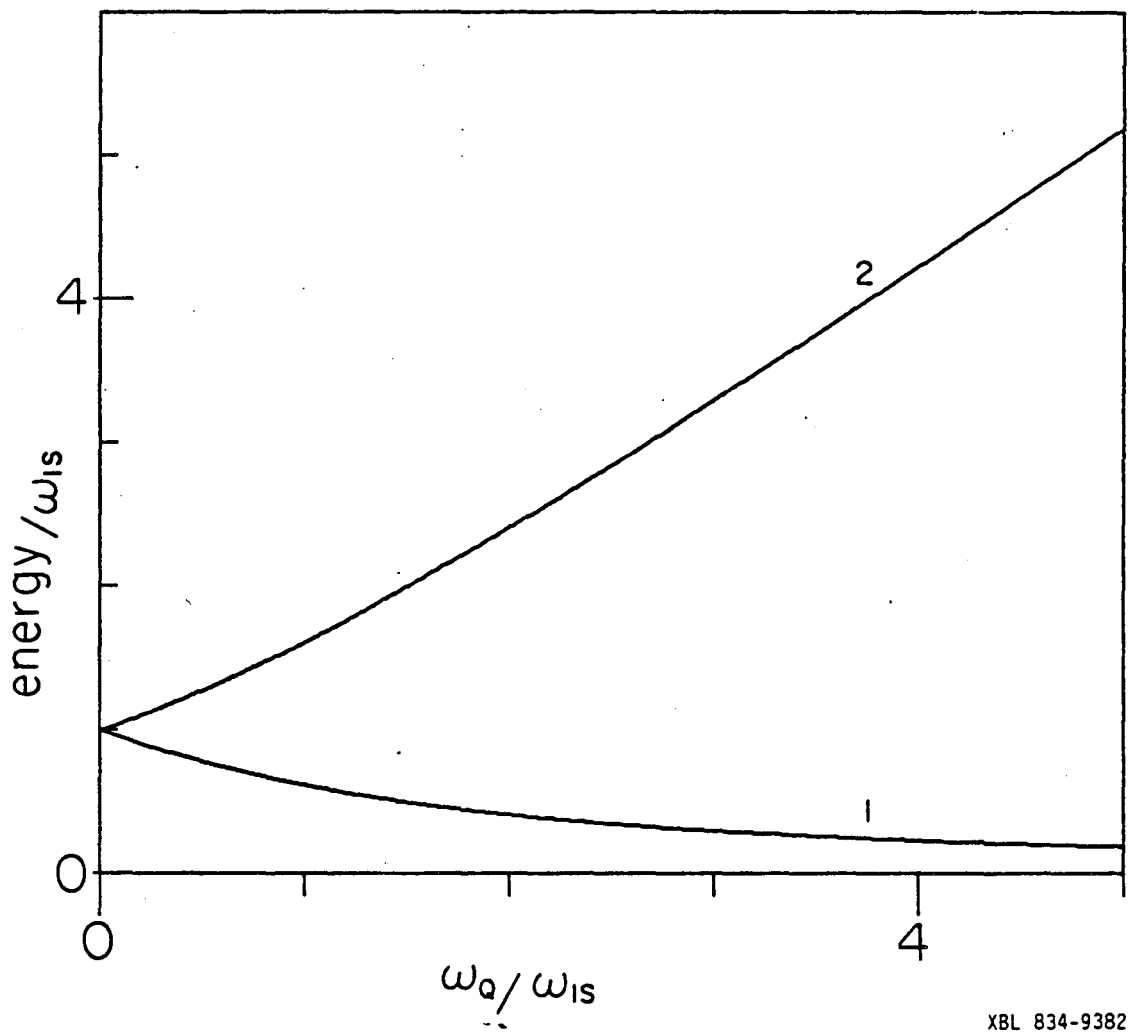

Figure 1b

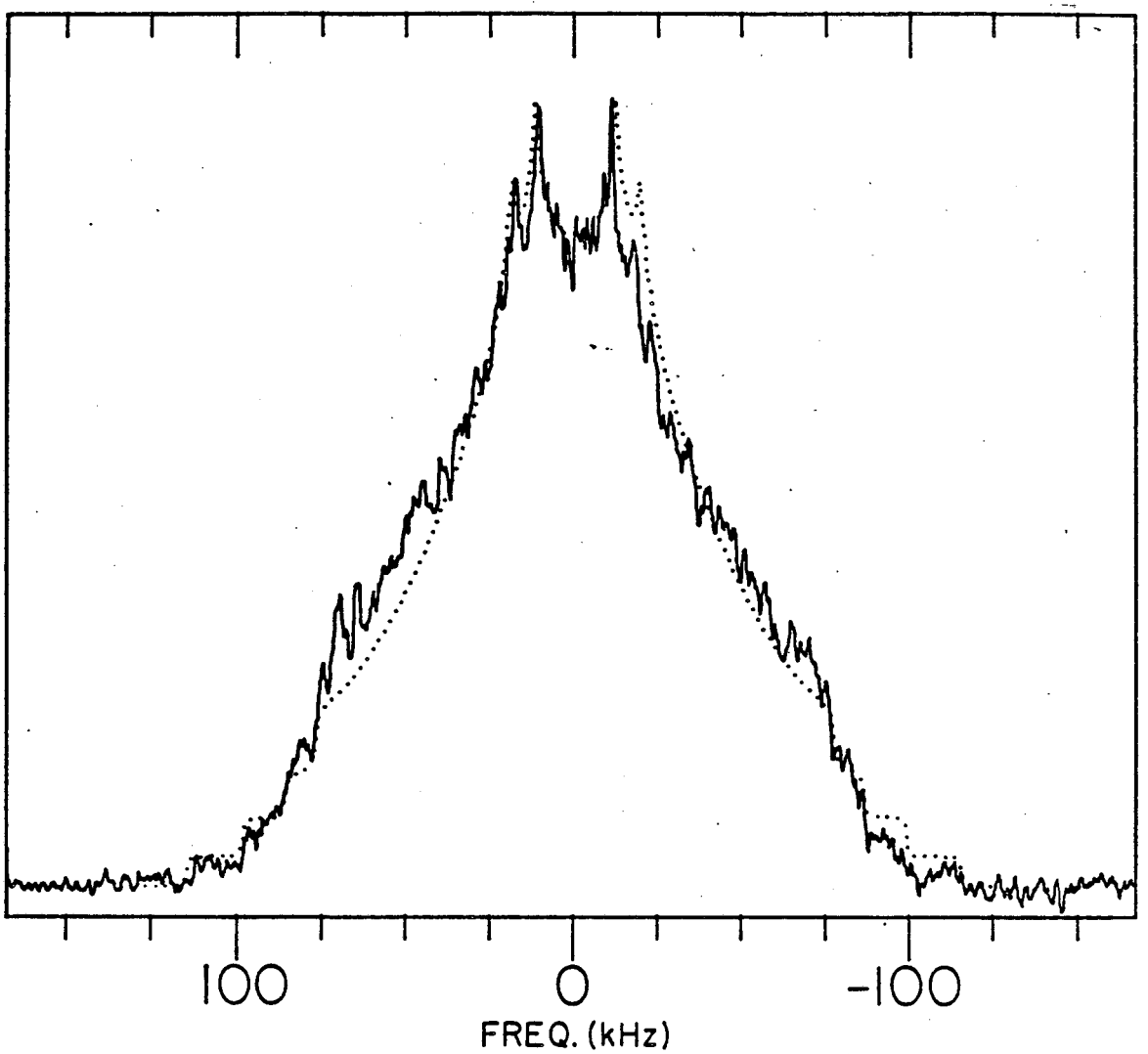

XBL 834-9391

Figure 2

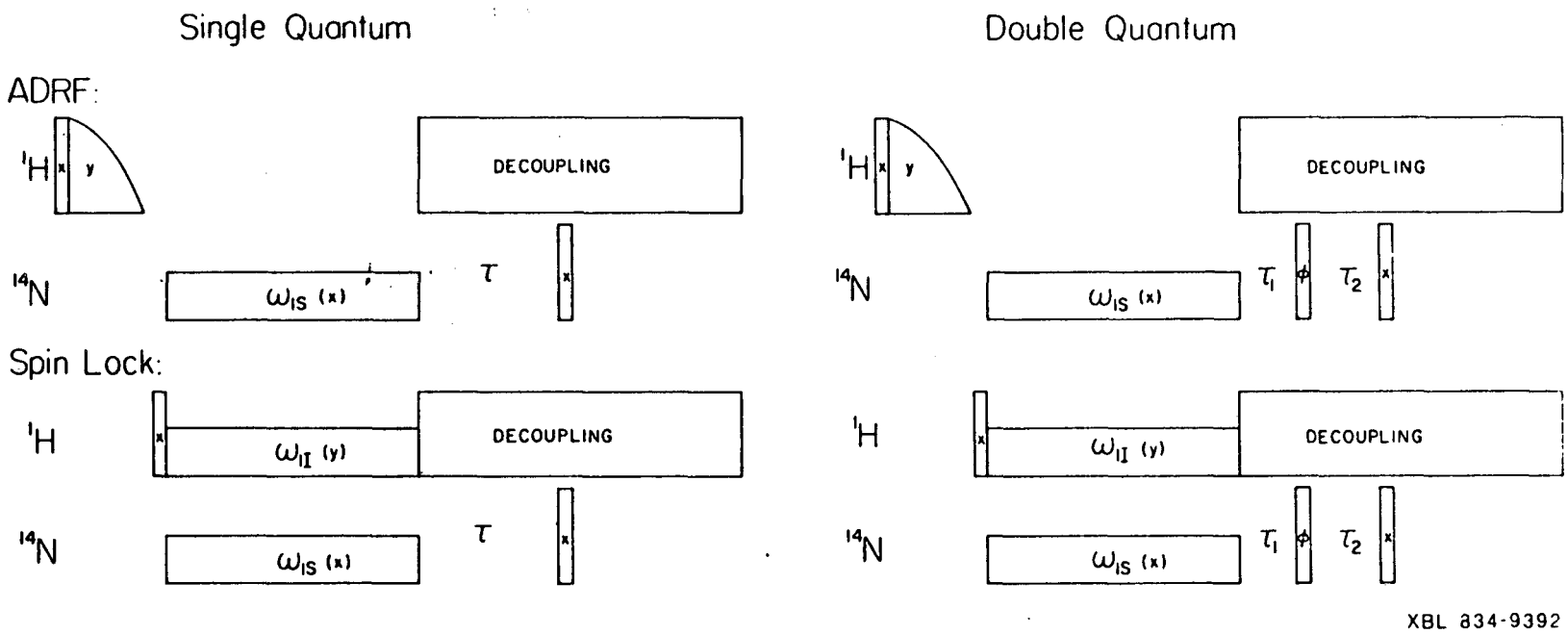
Single Quantum
Double Quantum
ADRF:
^1H
x
y
DECOUPLING
^{14}N
ω_{IS} (x)
τ
τ_1
τ_2
Spin Lock:
^1H
ω_{II} (y)
^{14}N
ω_{IS} (x)
XBL 834-9392

Figure 3

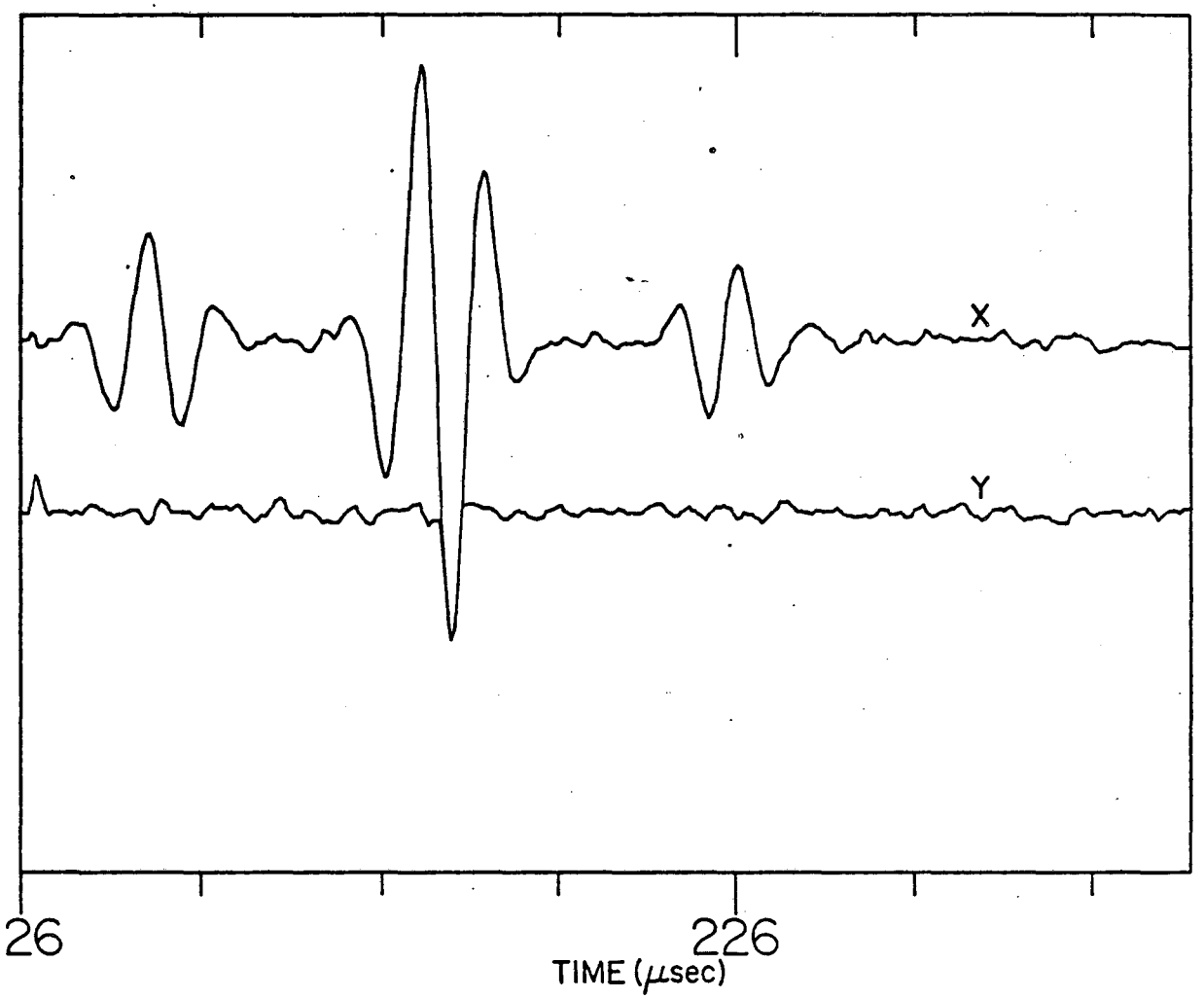

XBL 834-9385

Figure 4a

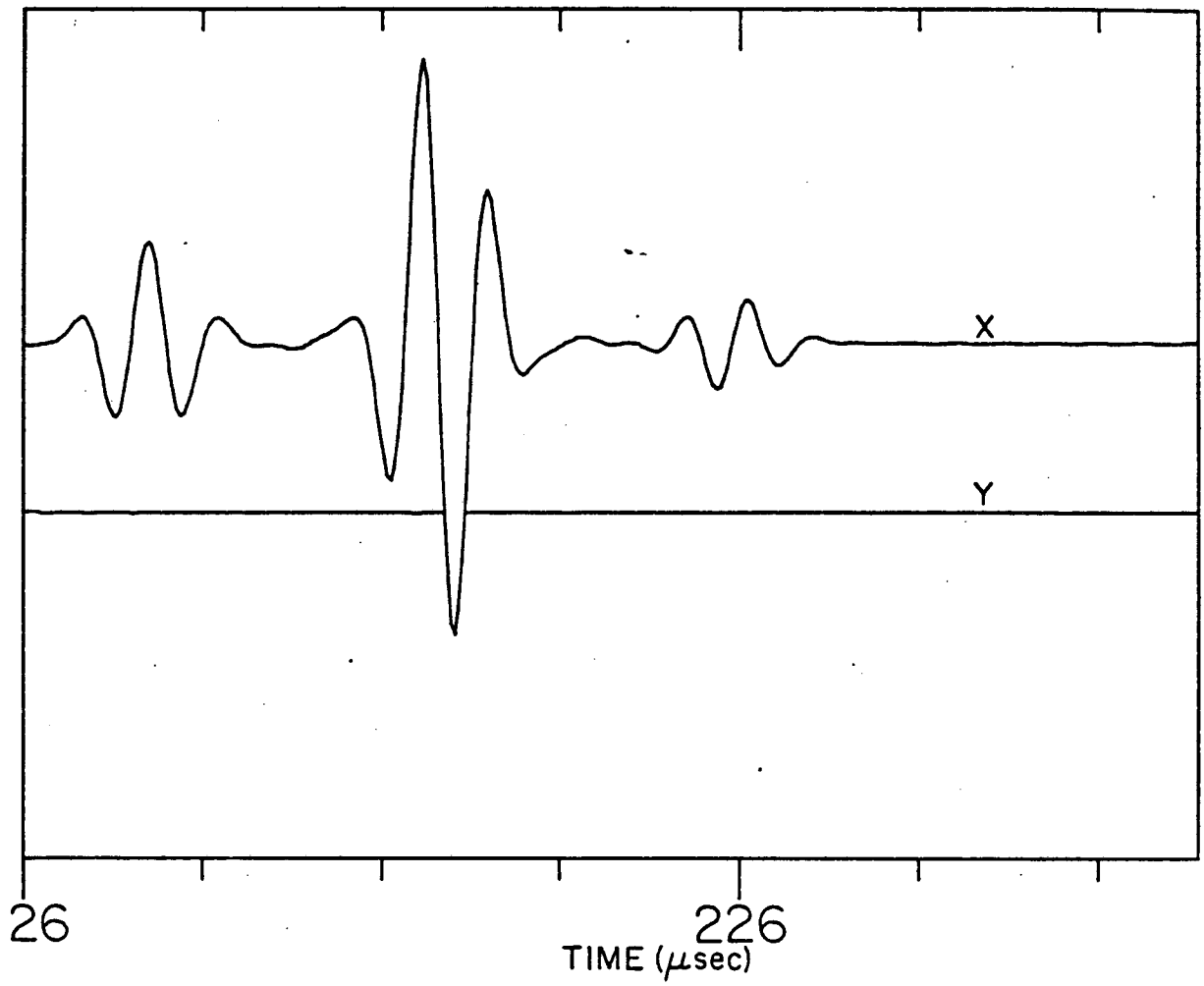

Figure 4b

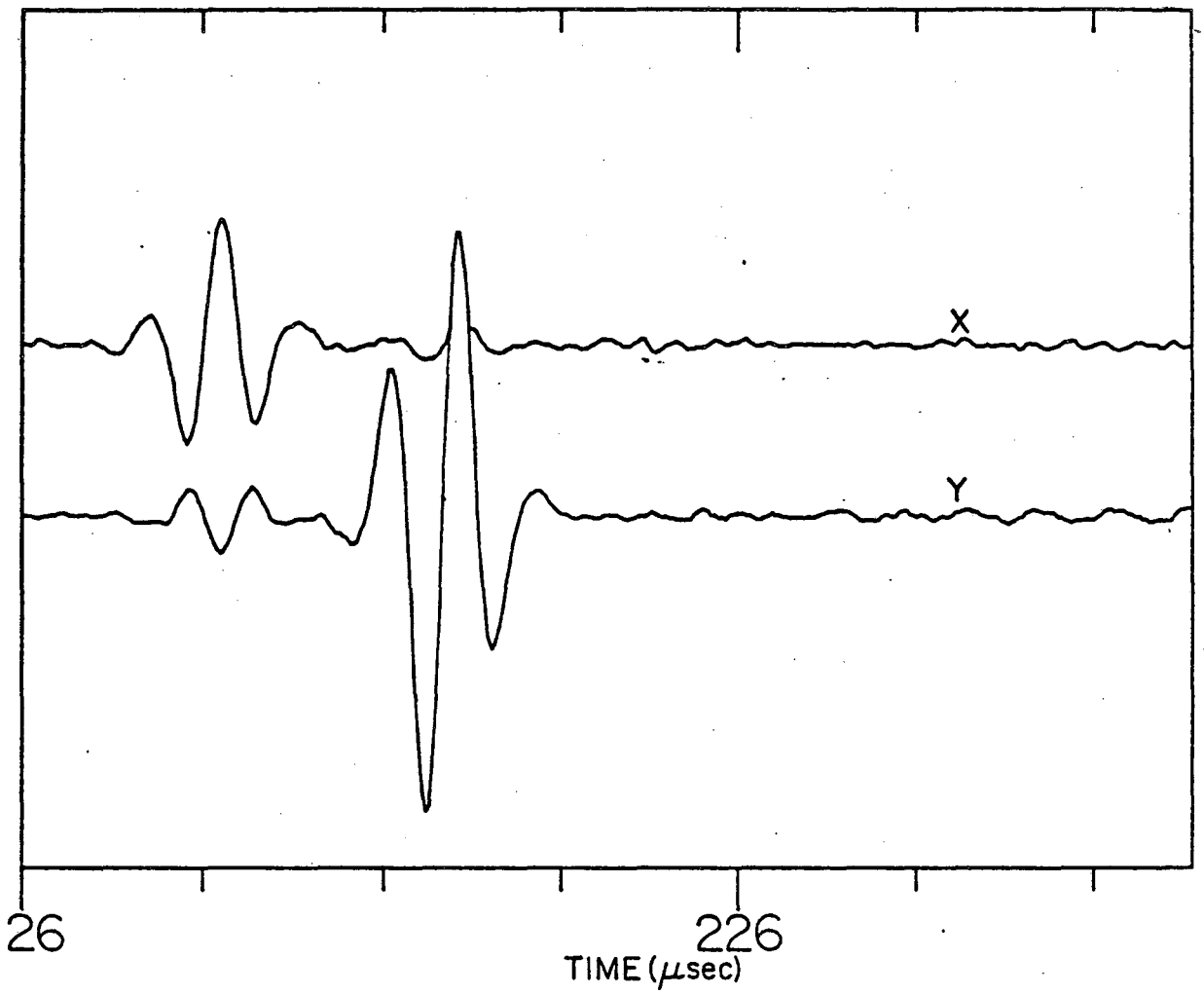

XBL 834-9386

Figure 4c

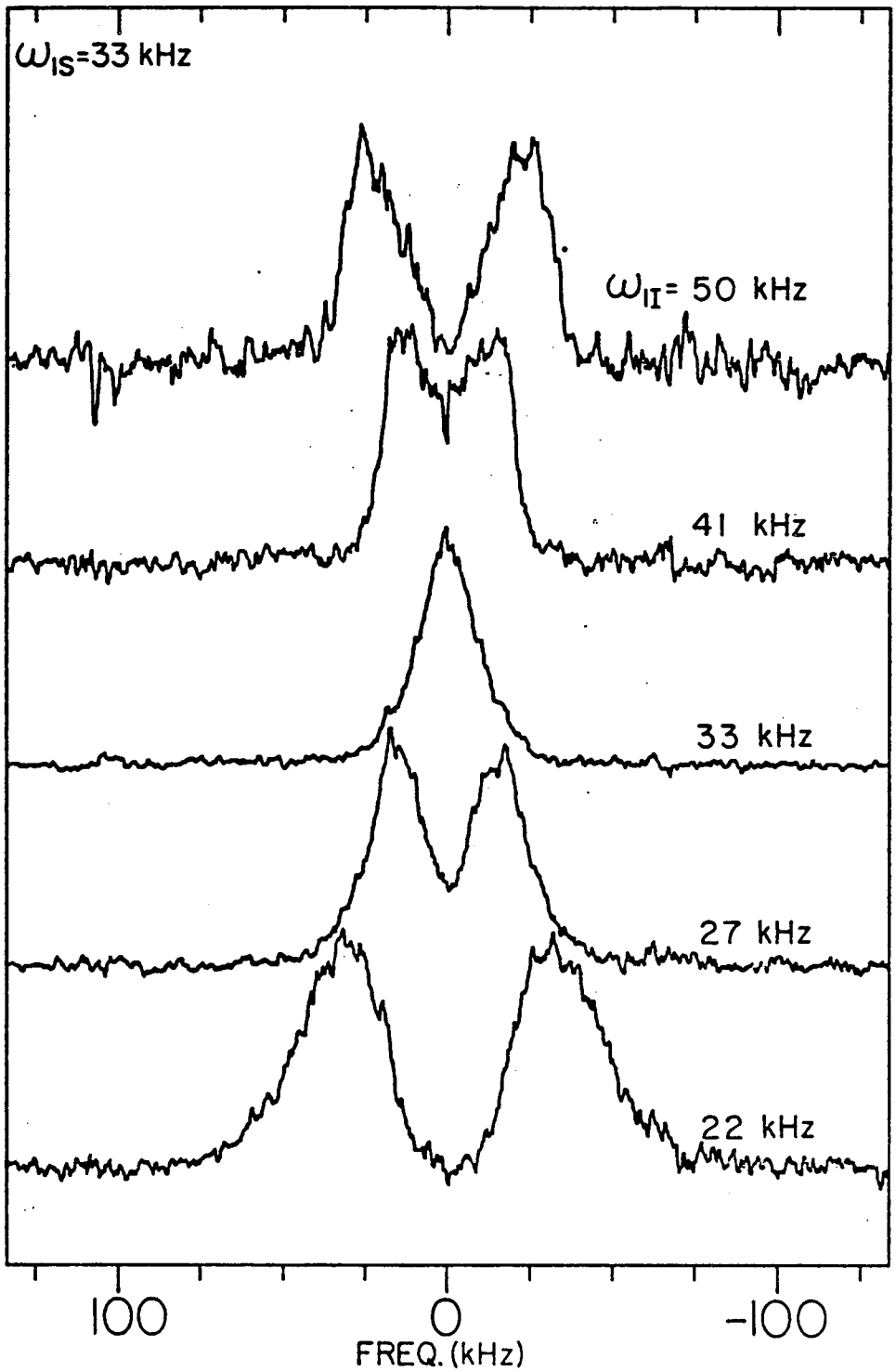

XBL 834-9387

Figure 5

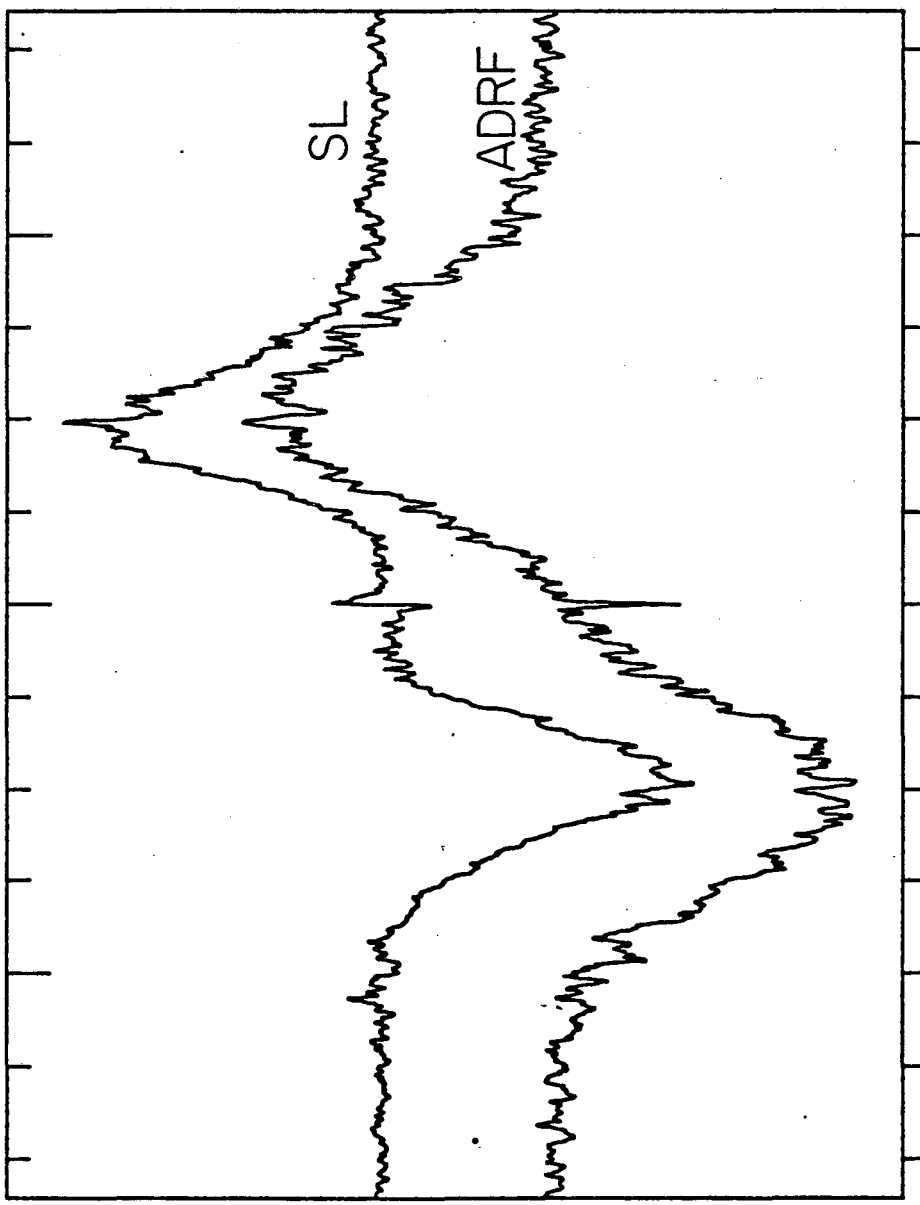

XBL 834-9405

Figure 6

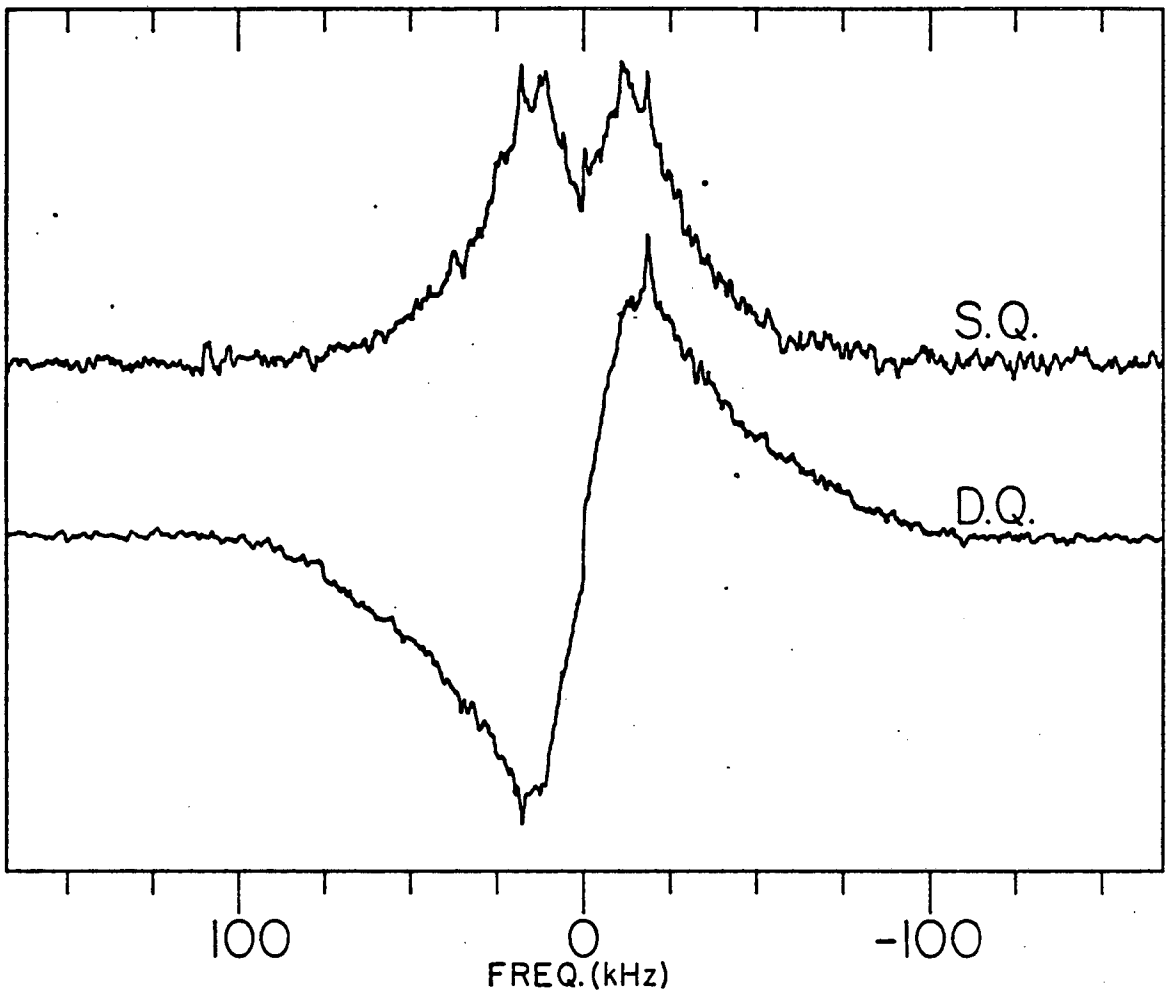

XBL 834-9388

Figure 7

Figure 8

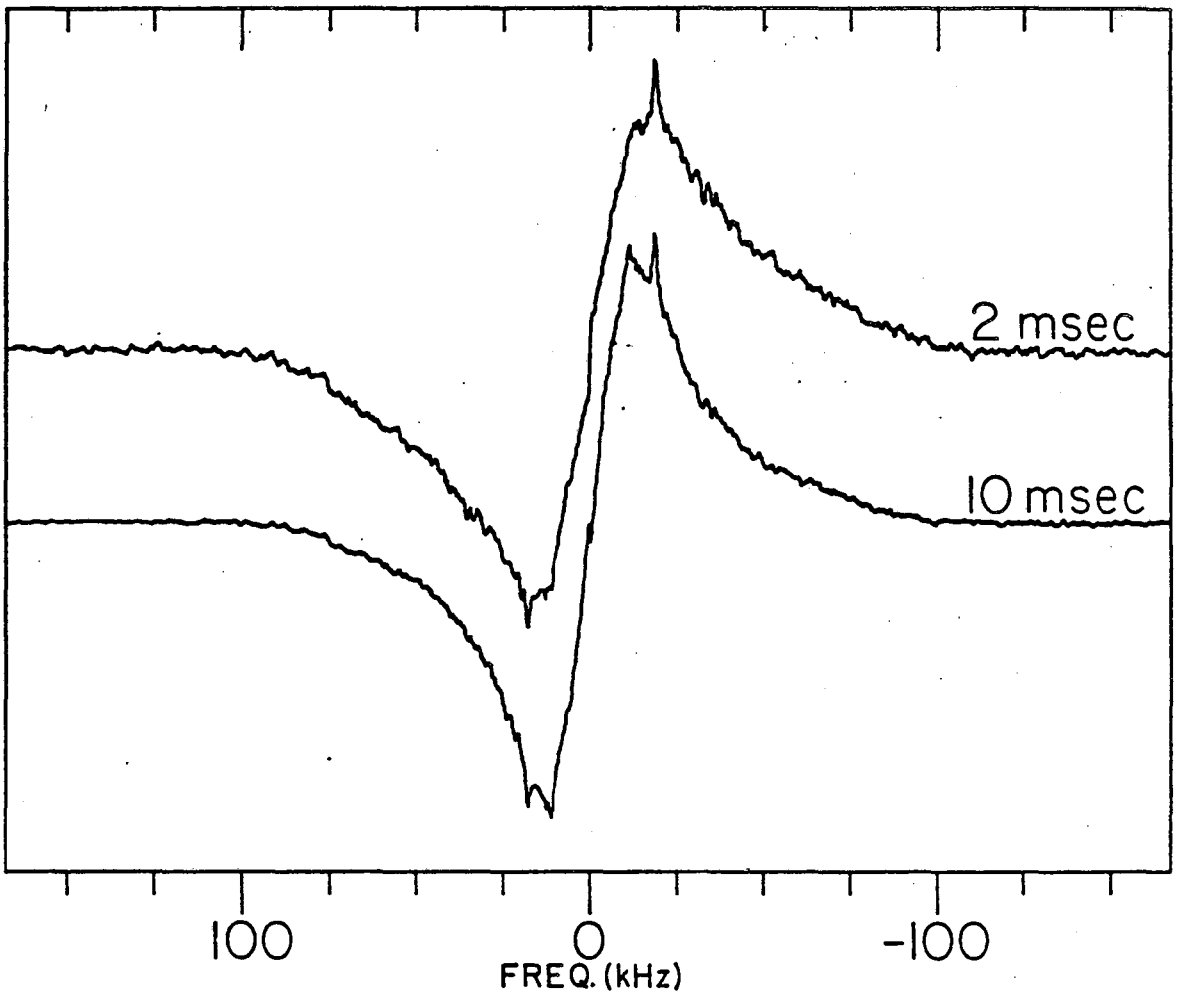

XBL 834-9389

Figure 9a

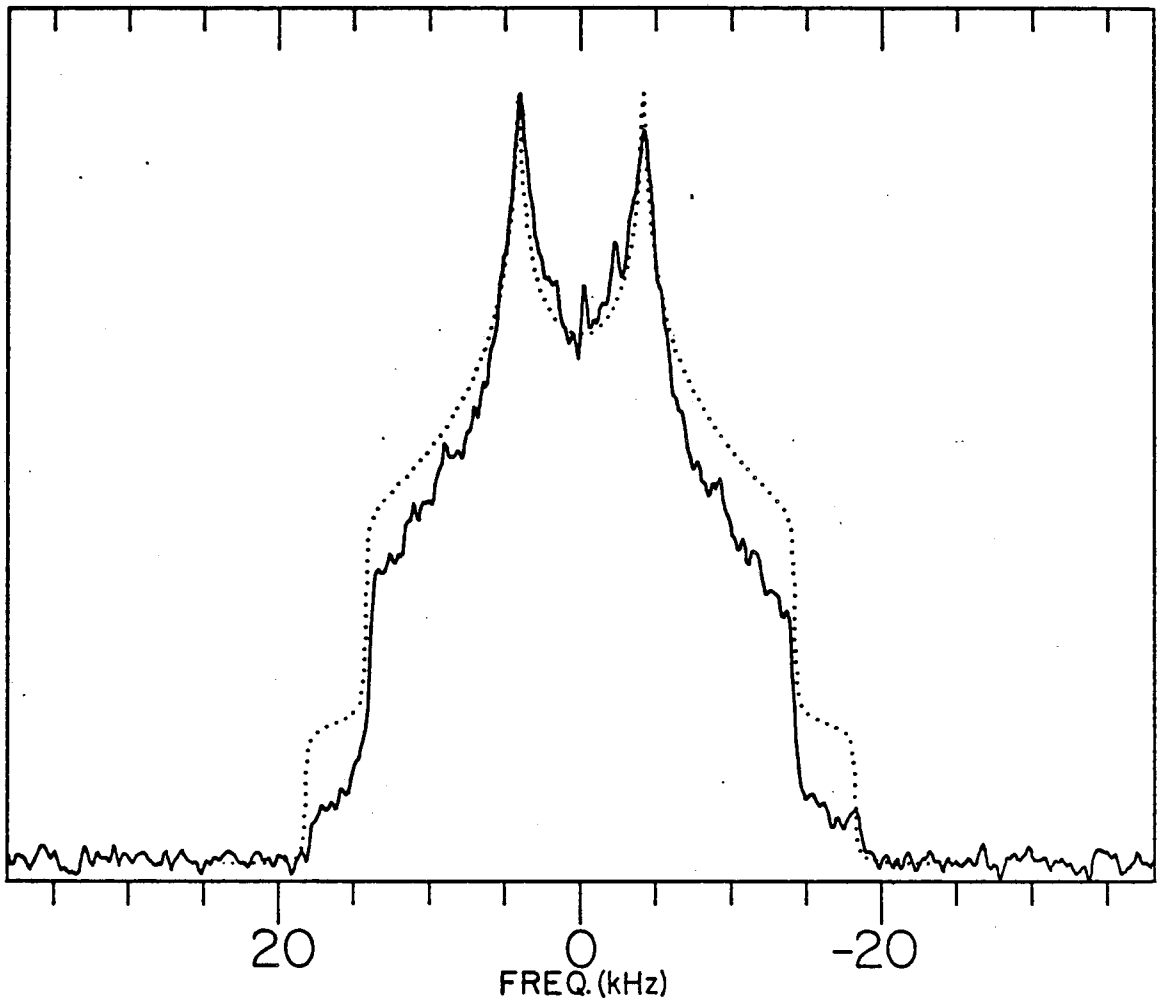

XBL 834-9381

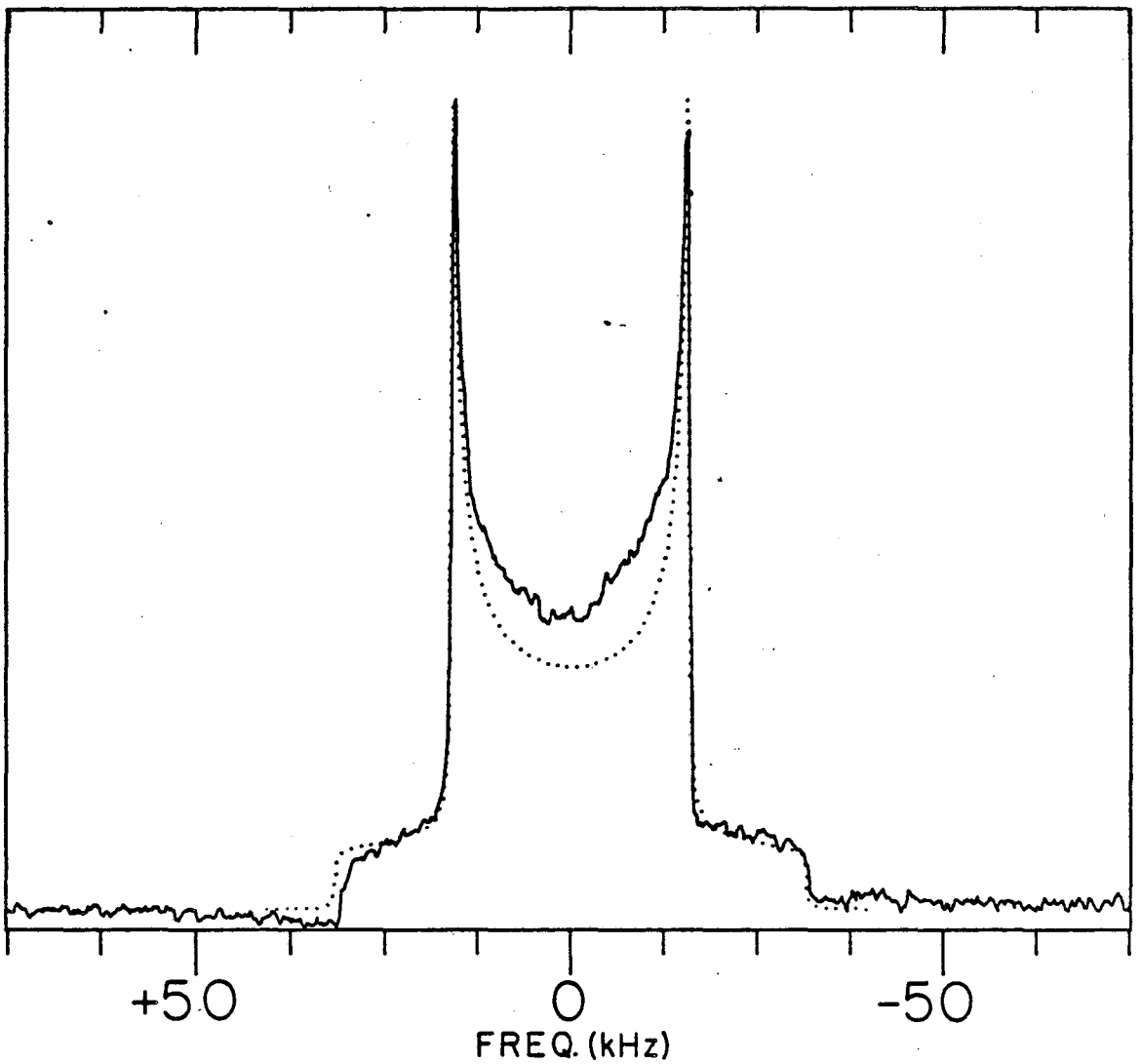

XBL 831-7631

Figure 9c

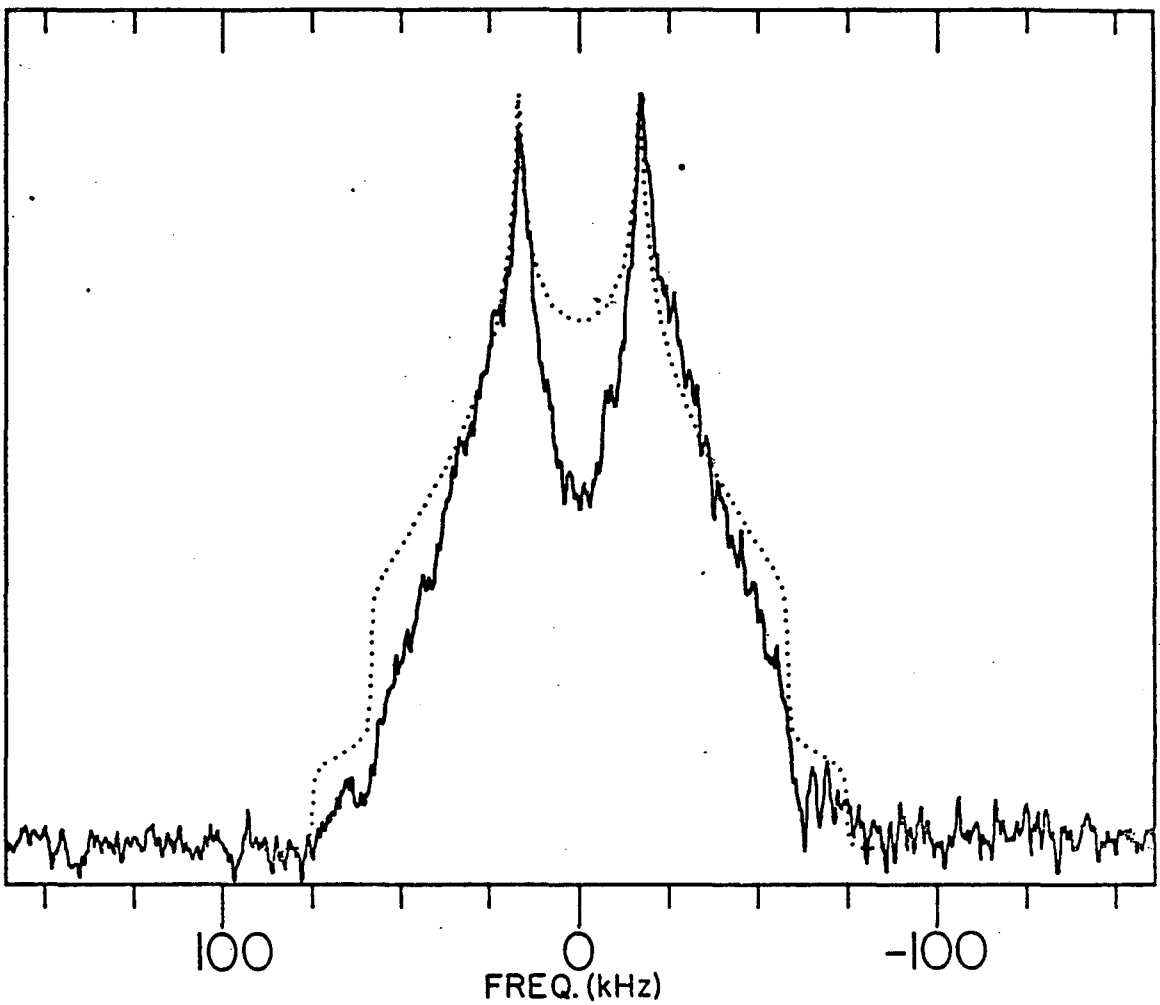

XBL 834-9390

TECHNICAL INFORMATION DEPARTMENT
LAWRENCE BERKELEY LABORATORY
UNIVERSITY OF CALIFORNIA
BERKELEY, CALIFORNIA 94720